CHEMISTRY
A EUROPEAN JOURNAL

FULL PAPER

DOI: 10.1002/chem.201103701

The Exohedral Diels–Alder Reactivity of the Titanium Carbide Endohedral Metallofullerene $Ti_2C_2@D_{3h}$-C_{78}: Comparison with D_{3h}-C_{78} and $M_3N@D_{3h}$-C_{78} (M = Sc and Y) Reactivity

Marc Garcia-Borràs,[a] Sílvia Osuna,[c] Josep M. Luis,*[a] Marcel Swart,*[a, b] and Miquel Solà*[a]

Abstract: The chemical functionalization of endohedral (metallo)fullerenes has become a main focus of research in the last few years. It has been found that the reactivity of endohedral (metallo)fullerenes may be quite different from that of the empty fullerenes. Encapsulated species have an enormous influence on the thermodynamics, kinetics, and regiochemistry of the exohedral addition reactions undergone by these species. A detailed understanding of the changes in chemical reactivity due to incarceration of atoms or clusters of atoms is essential to assist the synthesis of new functionalized endohedral fullerenes with specific properties. Herein, we report the study of the Diels–Alder cycloaddition between 1,3-butadiene and all nonequivalent bonds of the $Ti_2C_2@D_{3h}$-C_{78} metallic carbide endohedral metallofullerene (EMF) at the BP86/TZP//BP86/DZP level of theory. The results obtained are compared with those found by some of us at the same level of theory for the D_{3h}-C_{78} free cage and the $M_3N@D_{3h}$-C_{78} (M = Sc and Y) metallic nitride EMFs. It is found that the free cage is more reactive than the $Ti_2C_2@D_{3h}$-C_{78} EMF and this, in turn, has a higher reactivity than $M_3N@D_{3h}$-C_{78}. The results indicate that, for $Ti_2C_2@D_{3h}$-C_{78}, the corannulene-type [5,6] bonds **c** and **f**, and the type B [6,6] bond **3** are those thermodynamically and kinetically preferred. In contrast, the D_{3h}-C_{78} free cage has a preference for addition to the [6,6] **1** and **6** bonds and the [5,6] **b** bond, whereas $M_3N@D_{3h}$-C_{78} favors additions to the [6,6] **6** (M = Sc) and [5,6] **d** (M = Y) bonds. The reasons for the regioselectivity found in $Ti_2C_2@D_{3h}$-C_{78} are discussed.

Keywords: bond theory · cage compounds · cycloaddition · fullerenes · regioselectivity

Introduction

The detection of the first stable endohedral metallofullerene (EMF), $La@C_{60}$, was accomplished only a few months after the discovery of C_{60}.[1] Nowadays it is well known that fullerenes can encapsulate atoms, ions, metallic clusters, and small molecules such as H_2, CO, H_2O, NH_3, or CH_4 (for reviews see reference [2]). These endohedral fullerenes (EFs) can be classified in different groups:[2d] 1) classical EFs of the type $X@C_{2n}$, $X_2@C_{2n}$, and $X_3@C_{2n}$, with X = metal, noble gas, or small molecule, and $60 \leq 2n \leq 88$); 2) metallic nitride EMFs such as $M_3N@C_{2n}$, with M = metal and $68 \leq 2n \leq 96$; 3) metallic carbide EMFs like $M_2C_2@C_{2n}$, $M_3C_2@C_{2n}$, $M_4C_2@C_{2n}$, hydrogenated metallic carbide $M_3CH@C_{2n}$, and metallic nitrogen carbide $M_3CN@C_{2n}$ with $68 \leq 2n \leq 92$; 4) metallic oxide EMFs of the type $M_4O_2@C_{2n}$ and $M_4O_3@C_{2n}$; and 5) metallic sulfide $M_2S@C_{2n}$.

The synthesis and characterization of metallic carbide EMFs represents one of the most active areas of current research in fullerene chemistry. These species have interesting physicochemical properties with many potential interesting applications in the fields of magnetism, superconductivity, nonlinear optical (NLO) properties, radioimmunotherapy, and magnetic resonance imaging (MRI) contrast agents, among others. In 2001, Shinohara et al. characterized the first metal carbide EMF, $Sc_2C_2@C_{84}$.[3] In fact, this scandium carbide EMF was synthesized by the same group two years previously but it was erroneously assigned as $Sc_2@C_{86}$.[4] Incorrect assignments have been recurrent in the field of metal carbide EMFs due to the experimental difficulties present in the characterization of these compounds that are obtained generally in low yield and are often difficult to isolate. Thus, for instance, Sc_2C_{84}, Sc_3C_{82}, and Y_2C_{84}, which

[a] M. Garcia-Borràs, Dr. J. M. Luis, Prof. M. Swart, Prof. M. Solà
Institut de Química Computacional and Departament de Química
Universitat de Girona
Campus Montilivi, 17071 Girona, Catalonia (Spain)
E-mail: josepm.luis@udg.edu
miquel.sola@udg.edu

[b] Prof. M. Swart
Institució Catalana de Recerca i Estudis Avançats (ICREA)
Pg. Lluís Companys 23, 08010 Barcelona, Catalonia (Spain)
E-mail: marcel.swart@icrea.cat

[c] Dr. S. Osuna
Department of Chemistry and Biochemistry
University of California, Los Angeles
607 Charles E. Young Drive, Los Angeles, CA 90095 (USA)

Supporting information for this article is available on the WWW under http://dx.doi.org/10.1002/chem.201103701.

were at first considered to be classical EFs of the type $M_2@C_{2n}$ and $M_3@C_{2n}$, were finally classified as the metal carbide EMFs $Sc_2C_2@C_{82}$, $Sc_3C_2@C_{80}$, and $Y_2C_2@C_{82}$, respectively.[5] On the other hand, neither Y_2C_{82} nor Y_3C_{80} was found to be a metal carbide EMF and they were assigned to be $Y_2@C_{82}$ and $Y_3@C_{80}$ classical EFs.[5c,6] Interestingly, the initially assigned $Ti_2@C_{80}$ was found to be $Ti_2C_2@D_{3h}(78:5)$-C_{78} by ^{13}C NMR spectroscopy and density functional theory (DFT) calculations.[7] The $D_{3h}(78:5)$-C_{78} cage in $Ti_2C_2@D_{3h}(78:5)$-C_{78} represents the smallest fullerene cage obeying the isolated pentagon rule (IPR) that has a metal carbide encapsulated. For non-IPR cages, the smallest metal carbide disclosed so far is $Sc_2C_2@C_{68}$.[8] From an electronic point of view, metal carbides can formally transfer four electrons to the fullerene cage as in $(Sc_2C_2)^{4+}@(C_{82})^{4-}$ or six electrons like in $(Ti_2C_2)^{6+}@(C_{78})^{6-}$ or $(Sc_3C_2)^{6+}@(C_{80})^{6-}$.[9]

Organic functionalization of EMFs is an important research direction for the synthesis of novel materials with finely tuned properties. Tremendous efforts have been devoted to the functionalization of EMFs and to get a better understanding of their reactivity. Nevertheless, studies of regioselectivity in cycloaddition reactions to EMFs are still scarce. The main reason is the difficulty in producing and isolating sufficient quantities to investigate their reactivity. In fact, the low EMF yields limit investigations on the EMFs' reactivity to mainly the most abundant, that is, classical EFs with the C_{82} cage and $Sc_3N@C_{80}$. To date, only a couple of reactivity studies have been devoted to metal carbide EMFs. In 2007, Iiduka et al.[10] synthesized $Sc_2C_2@C_{82}$(Ad) from the reaction of $Sc_2C_2@C_{82}$ (isomer III) with 2-adamantane-2,3-[3*H*]-diazirine. The product corresponds with the addition to a [5,6] bond and has an open structure. On the other hand, the relatively large HOMO–LUMO gap calculated for $Sc_2C_2@C_{82}$ of 2.01 eV justified the low reactivity of $Sc_2C_2@C_{82}$ towards disilirane.[11] More recently, Wang and co-workers have synthesized a $Sc_3C_2@C_{80}$ fulleropyrrolidine monoadduct.[12] The [5,6] ring junction was also found to be the reactive site for the Prato reaction between $Sc_3C_2@C_{80}$ and *N*-ethylglycine in *ortho*-dichlorobenzene.[12]

As discussed in a recent review,[13] theoretical studies are important to predict or to give support to experimental results on addition sites. What is more, these studies offer clues to understand the origin of the regioselectivity in EMFs.[2a,13] In the past, we analyzed the regiochemistry of $M_3N@D_{3h}(78:5)$-C_{78} (M = Sc and Y) metallic nitride EMFs in comparison with that of free $D_{3h}(78:5)$-C_{78}.[14] In particular, we studied the Diels–Alder (DA) reaction of 1,3-butadiene in the s-*cis* conformation with all nonequivalent bonds of free and M_3N-encapsulated $D_{3h}(78:5)$-C_{78}. It was found that the regiochemistry changes dramatically when the cluster is encapsulated inside. Thus, whereas for free C_{78} the preferred attack is at the type D [5,6] bond **b** (see Figures 1 and 2), in $Sc_3N@D_{3h}$-C_{78} the addition occurs preferentially at the type B [6,6] bond **6** and for $Y_3N@D_{3h}$-C_{78} at the type D [5,6] bond **d**.

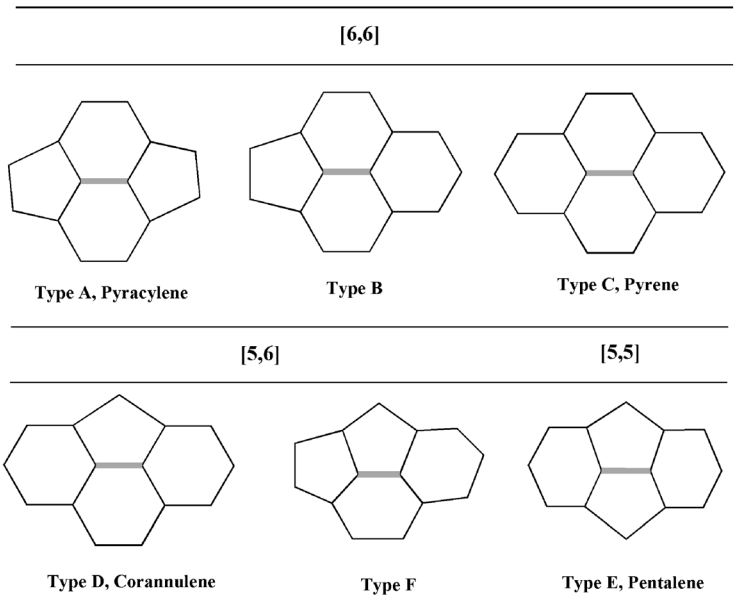

Figure 1. Representation of the different [6,6], [5,6], and [5,5] bond types that may be present in any fullerene structure.

It was clear from these studies that the interaction between the encapsulated species and the carbon cage leads to important changes not only in the reactivity but also in the regiochemistry of the fullerene cages. It should be noted that EMFs are in general less reactive than their respective free cages, and usually the cage does not correspond to the most stable isomer for the free species. In the present work we aim to extend these previous studies to $Ti_2C_2@D_{3h}(78:5)$-C_{78}. The same reaction on all nonequivalent bonds of the fullerene cage will be analyzed at the same level of theory to make possible proper comparisons with previous results. There are several aspects that suggest that the regiochemistry in $Ti_2C_2@D_{3h}(78:5)$-C_{78} may show important changes compared to that of $M_3N@D_{3h}(78:5)$-C_{78} species. First, although formal transfer is the same in $Ti_2C_2@D_{3h}$-C_{78} and $M_3N@D_{3h}$-C_{78}, the actual charge transfer from the cluster to the fullerene will be different. It is well known that different amounts of charge transfer can change the regioselectivity of EMFs.[9] Second, the metals of the two clusters inside the $D_{3h}(78:5)$-C_{78} cage point to different sites of the fullerene (Ti_2C_2 is parallel to the C_3 axis and the M_3N is perpendicular to this axis, see Figure 2), so it is likely that the charge transfer from the HOMOs of the cluster would involve different LUMOs of the fullerene and this may have an important effect on the reactivity of the different bonds. And finally, due to the different orientation of the two clusters, the deformation of the cage and the locations of the more strained sites are different, which may also induce major changes in the chemical reactivity of the analyzed EMFs. Thus, the main goal of the present work is to investigate these issues by comparing the regiochemistry of $Ti_2C_2@D_{3h}(78:5)$-C_{78} with that of free and trimetallic nitride template (TNT) M_3N (M = Sc and Y) encapsulated C_{78}.

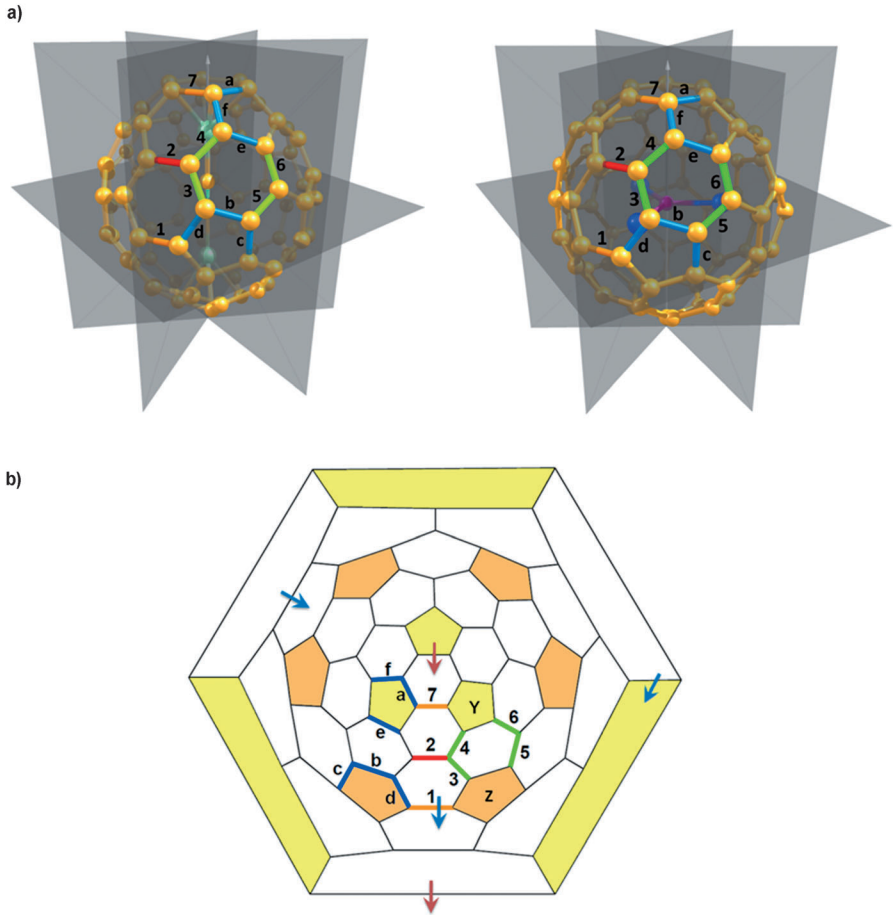

Figure 2. a) The different nonequivalent bonds of $Ti_2C_2@C_{78}$ are represented, in which numbers denote [6,6] bonds and lowercase letters [5,6] bonds. Different colors are used to mark the different bond types (orange, type A; green, type B; red, type C; blue, type D). b) Schlegel diagram of $Ti_2C_2@C_{78}$, which converts the 3D fullerene structure into a 2D representation. The positions of the titanium atoms facing the different bonds are symbolized by a red arrow. For comparison the same information is given for $Sc_3N@C_{78}$, where blue arrows are used to indicate the position of scandium atoms in the Schlegel diagram. The two types of nonequivalent five-membered rings are marked in yellow for type **Y** (formed by **f**, **a**, **f**, **e**, and **e** bonds) and orange for type **Z** (formed by **b**, **c**, **b**, **d**, and **d** bonds).

Computational Details

All DFT calculations were performed with the Amsterdam density functional (ADF) program.[15] The molecular orbitals (MOs) were expanded in an uncontracted set of Slater-type orbitals (STOs) of double-ζ (DZP) and triple-ζ potential (TZP) quality containing diffuse functions and one set of polarization functions. To reduce the computational time needed to carry out the calculations, the frozen core approximation was used.[15a] In this approximation, the core density is obtained and included explicitly, albeit with core orbitals that are kept frozen during the self-consistent field (SCF) procedure. Therefore, in this work core electrons (1s for 2nd period, 1s2s2p for 3rd and 4th period) were kept frozen during the geometry optimizations (frozen core approximation),[15a] as it was shown to have a negligible effect on the obtained geometries.[16] For a proper comparison with previous studies,[14] scalar relativistic corrections were included self-consistently by using the zeroth-order regular approximation (ZORA).[17] An auxiliary set of s, p, d, f, and g STOs was used to fit the molecular density and to represent the Coulomb and exchange potentials accurately for each SCF cycle.[18] Energies and gradients were calculated by using the local density approximation (Slater exchange and VWN correlation[19]) with nonlocal corrections for exchange (Becke88)[20] and correlation (Perdew86)[21] included self-consistently (i.e., the BP86 functional). All energies reported herein were obtained with the TZP basis in single-point energy calculations at geometries that were obtained with the DZP basis (i.e., BP86/TZP//BP86/DZP). It is well documented that standard DFT functionals such as BP86 underestimate energy barriers[22] (in the case of the DA reaction between ethene and 1,3-butadiene in the s-*cis* conformation, BP86/TZP predicts a barrier of 18.6 kcal mol^{-1}, that is, an underestimation of the experimental value by about 6 kcal mol^{-1}). Nevertheless, we expect that all DA reactions studied herein will suffer very similar underestimations.

The actual geometry optimizations and transition state (TS) searches were performed with the QUILD[23] (QUantum regions Interconnected by Local Descriptions) program, which functions as a wrapper around the ADF program. The QUILD program constructs all input files for ADF, runs ADF, and collects all data; ADF is used only for the generation of the energy and gradients. Furthermore, the QUILD program uses improved geometry optimization techniques, such as adapted delocalized coordinates[24] and specially constructed model Hessians with the appropriate number of eigenvalues.[24] The latter is of particular use for TS searches. All TSs were characterized by computing the analytical[25] vibrational frequencies, to have one (and only one) imaginary frequency corresponding to the approach of the two reacting carbon atoms.

Pyramidalization angles, introduced by Haddon[26] as a measure of the local curvature in polycyclic aromatic hydrocarbons, were calculated by using the POAV3 program.[27] Energy dispersion corrections were introduced by using Grimme's methodology[28] (D_3) implemented in the ADF 2010.01 version.[15b] Only the initial complexes were fully optimized by using these corrections in each optimization step. Dispersion corrections for the other structures were included by single-point calculations on the stationary-point structure found in a usual optimization procedure (i.e., BP86-D_3/TZP//BP86/DZP). We did not reoptimize all structures as differences in structural parameters were minimal. Some of us have recently shown that dispersion corrections are essential for a correct description of the thermodynamics and kinetics of fullerene and nanotube reactions.[29]

Results and Discussion

We have analyzed the change in reactivity and regioselectivity induced by the encapsulated metallic cluster Ti_2C_2 in the DA reaction with 1,3-butadiene in the s-*cis* conformation. Seven [6,6] and six [5,6] nonequivalent bonds are studied to

take into account all possible final reaction products (see Figure 2).

Molecular and electronic structure of $Ti_2C_2@D_{3h}$-C_{78}: First of all, we studied the location of the acetylide (C_2) group in the cluster. The two Ti atoms were placed on the C_3 axis that goes through the centers of the top and bottom hexagon and restrained to stay on that axis (but allowed to move freely up and down along the axis). For the C_2^{2-} moiety between the two Ti atoms inside the D_{3h}-C_{78} cage three different orientations are possible (see Figure 3). The BP86/TZP// BP86/DZP results indicate that the linear (end-on) configuration is more stable than the zigzag one by only 0.4 kcal mol^{-1}, whereas the butterfly (side-on) configuration lies about 22 kcal mol^{-1} higher in energy. These results are qualitatively in agreement with previous B3LYP/6-31G(d) calculations indicating that the end-on isomer is 38.3 kcal mol^{-1} lower in energy than the side-on isomer and that the energy barrier that has to be surmounted for the conversion of the end-on to the side-on isomer is 48.7 kcal mol^{-1}.[7e] The large energy barrier and energy difference clearly support the end-on bridge mode. Perdew–Burke–Ernzerhof (PBE)/ double numerical polarized (DNP) calculations also favor the end-on conformer for Ti_2C_2 encapsulated in D_{3h}-C_{78}.[30] Moreover, end-on isomers were observed in transmission electron microscopy images of $Ti_2C_2@D_{3h}$-C_{78} encapsulated in single-walled nanotubes.[7e] Thus, one can conclude that the C_2^{2-} unit is located mainly in the direction of the C_3 axis and at room temperature can freely rotate between the end-on and zigzag conformations. For the end-on conformation, we also checked the possible rotation of Ti_2C_2 along two axes perpendicular to the C_3 axis and passing through the center of mass of the Ti_2C_2 cluster. To this end, we performed single-point energy calculations rotating 15° along these two perpendicular axes, while keeping the fullerene and the internal geometry of the cluster frozen. We have seen that such rotations are hindered by high energy barriers. Indeed a small rotation of 15° already requires about 80 kcal mol^{-1}. Consequently, we will perform our study starting from the end-on conformation, which is the lowest-energy structure, without taking into account possible rotations of the cluster. However, it should be noted that during optimizations of transition states, intermediates, products, and initial complexes we allow the cluster to freely move between the end-on and zigzag conformations.

The incarceration of the metallic cluster inside the fullerene cage has an important effect on many of the bond lengths of the 13 different bonds of the D_{3h}-C_{78} cage, as can be appreciated from Table 1. The changes in bond lengths are due to two effects. First, strain caused by the metal cluster elongates the bonds close to the metal atoms. Second, charge

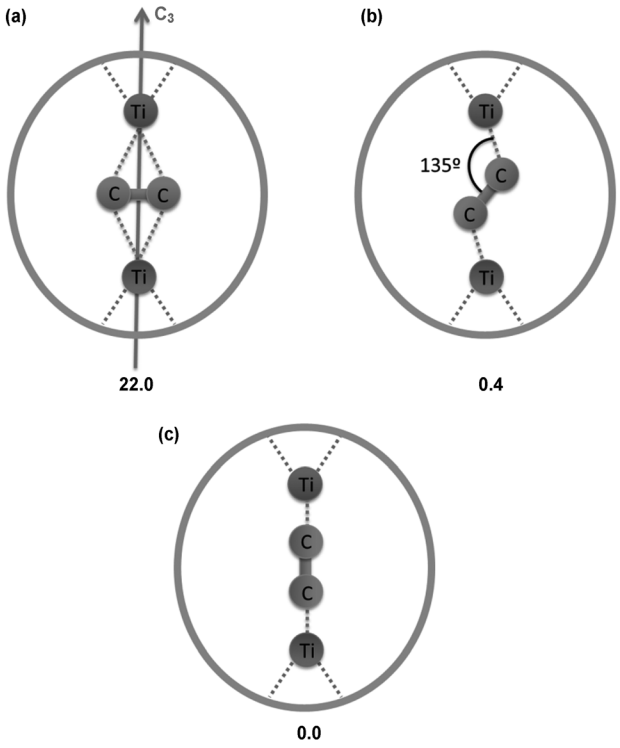

Figure 3. The three possible orientations of the acetylide unit in the D_{3h}-C_{78} cluster: a) butterfly or side-on, b) zigzag, and c) linear or end-on. Differences in stability referred to the end-on isomer are given in kcal mol^{-1}.

Table 1. BP86/DZP bond lengths R_{full} [Å] and pyramidalization angles θ_p [°] for free C_{78}. The differences in bond lengths ΔR_{full} [Å] and pyramidalization angles $\Delta\theta_p$ [°] between endofullerenes and the free C_{78} cage are also presented for all nonequivalent bonds. Reported pyramidalization angles represent the average over the two atoms that constitute the bond under consideration. Root mean square (RMS) values are calculated taking into account the total number of nonequivalent bonds.

	D_{3h}-C_{78}[a]		$Sc_3N@D_{3h}$-C_{78}[a]		$Y_3N@D_{3h}$-C_{78} up[a]		$Y_3N@D_{3h}$-C_{78} down[a]		$Ti_2C_2@D_{3h}$-C_{78}	
Bond	R_{full}	θ_p	ΔR_{full}	$\Delta\theta_p$	ΔR_{full}	$\Delta\theta_p$	ΔR_{full}	$\Delta\theta_p$	ΔR_{full}	$\Delta\theta_p$
1	1.369	10.46	0.071	3.340	0.094	3.570	0.094	3.570	0.019	0.560
2	1.465	8.58	0.001	−0.250	0.010	−0.120	0.009	−0.030	−0.009	0.340
3	1.432	9.62	0.018	−0.360	0.028	0.210	0.016	0.020	−0.019	0.090
4	1.415	9.60	0.011	−0.160	0.017	−0.380	0.020	−0.260	0.031	−0.945
5	1.418	9.53	0.014	−0.560	0.025	−0.970	0.025	−0.860	−0.002	0.215
6	1.420	9.44	−0.020	0.550	−0.024	0.220	−0.022	0.340	0.003	−0.765
7	1.388	11.64	0.012	−0.430	0.010	−0.470	0.013	−0.580	0.069	1.890
a	1.438	11.64	−0.001	−0.430	0.001	−0.470	0.002	−0.580	0.039	1.890
b	1.410	10.49	0.036	−0.760	0.045	−0.390	0.047	−0.600	0.037	0.165
c	1.465	10.32	−0.042	−1.050	−0.042	−1.300	−0.042	−1.300	−0.043	0.490
d	1.446	10.56	0.006	1.440	0.022	2.060	0.018	1.820	−0.015	0.200
e	1.438	10.38	0.011	0.540	0.016	0.220	0.015	0.320	−0.003	−1.745
f	1.442	11.13	−0.010	−0.250	−0.011	−0.550	−0.011	−0.540	0.010	−0.170
	all bonds		0.022	0.858	0.033	1.163	0.032	1.127	0.027	0.918
RMS	[6,6]		0.021	0.862	0.036	1.236	0.035	1.217	0.029	0.816
	[5,6]		0.022	0.847	0.029	1.091	0.029	1.038	0.026	0.996

[a] Values from ref. [14b].

transfer from the HOMOs of the metal cluster to the LUMOs of the fullerene enlarges those bonds with antibonding interactions in the LUMOs of the fullerene and shortens those with bonding combinations. The deformation of the fullerene cage due to encapsulation of the cluster (measured as the energy difference between the same D_{3h}-C_{78} cage at the geometry it has in the EMF and at the optimized geometry of the free fullerene) is an indication of the strain suffered by the cage. For Ti_2C_2, this deformation energy is 39.6 kcal mol^{-1} at the BP86/TZP//BP86/DZP level of theory, quite similar to that of $Sc_3N@D_{3h}$-C_{78} (32.2 kcal mol^{-1}).[14a] From these results, one can conclude that D_{3h}-C_{78} encapsulating Ti_2C_2 or Sc_3N is not especially strained. For Y_3N this deformation energy is significantly higher (67.5 kcal mol^{-1}).[14b] The higher strain in $Y_3N@D_{3h}$-C_{78} is also reflected by the RMS values corresponding to the changes in the bond lengths and pyramidalization angles when going from free C_{78} to the encapsulated species given in Table 1. As the deformation energies for $Ti_2C_2@C_{78}$ and $Sc_3N@C_{78}$ are similar, $Ti_2C_2@C_{78}$ reactivity will be compared mostly with that of $Sc_3N@C_{78}$ rather than with the more strained $Y_3N@C_{78}$ EMF. It is worth noting that for the TNT moieties, the fullerene cage is deformed within the horizontal symmetry plane; however, when titanium metallic carbide is introduced, the fullerene cage is deformed along the C_3 symmetry axis. This can be clearly seen in Figure 4, in which the structures of $Ti_2C_2@C_{78}$ and $Sc_3N@C_{78}$ have been superimposed.

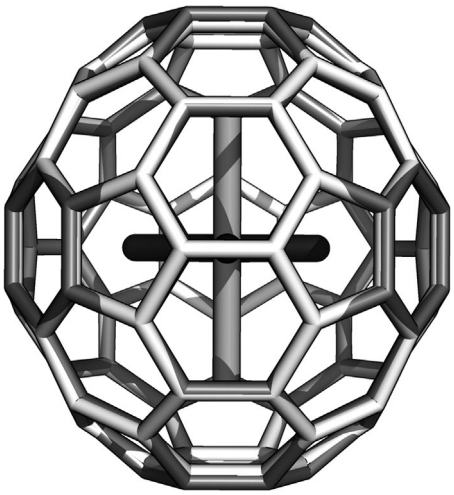

Figure 4. Representation of superimposed $Ti_2C_2@D_{3h}$-C_{78} (dark gray cage and light gray cluster) and $Sc_3N@D_{3h}$-C_{78} (light gray cage and dark gray cluster) EMFs.

As for the charge transfer, the Ti_2C_2 cluster donates fewer electrons to the cage than the Sc_3N cluster (Voronoi/Hirshfeld charges on the cluster are 0.60/0.53 and 0.98/0.82 for Ti_2C_2 and Sc_3N clusters, respectively). This results in a more reactive $Ti_2C_2@D_{3h}$-C_{78} EMF than $Sc_3N@D_{3h}$-C_{78}, which is in line with the fact that the LUMO energies of $Ti_2C_2@D_{3h}$-C_{78} and $Sc_3N@D_{3h}$-C_{78} are −4.49 and −3.87 eV, respectively. However, it is more interesting to analyze the frontier MOs of D_{3h}-C_{78} in Figure 5 and the MO diagram of Ti_2C_2 interacting with D_{3h}-C_{78} in Figure 6.

In the case of fullerene compounds, the main interaction occurs between the HOMO of butadiene (at −5.77 eV) and the LUMOs of the fullerene. In the $Ti_2C_2@D_{3h}$-C_{78} case, LUMO energies are found between −4.49 and −4.00 eV, and for the free C_{78} cage values go from −5.13 to −3.69 eV (see Figure 5). Note that because of the formal charge transfer upon metal-cluster encapsulation, the three LUMOs of the free fullerene are occupied and only higher-lying unoccupied orbitals are available for interaction with the HOMO of the diene. As a consequence, the HOMO(diene)–LUMO(fullerene) gap increases from 0.64 eV for free fullerene to 1.28 eV for the Ti_2C_2 EMF. This larger gap is an indication of a more stable and less reactive species. For comparison purposes the HOMO–LUMO gap in $Sc_3N@D_{3h}$-C_{78} is 1.57 eV.[14a]

As can be seen in Figure 6, the LUMOs of the free fullerene that interact more strongly with the HOMOs of the cluster are the degenerate LUMO+1 (E′). The six electrons transferred from the titanium cluster to the fullerene cage are placed in the three LUMOs of the fullerene (A_2' and E′), the A_2' orbital becoming the HOMO of the final complex because of the larger stabilization of the E′ MOs. Interestingly, in the $Sc_3N@C_{78}$ compound, the A_2' was much more stabilized than the E′ orbitals which were the HOMOs.[14a] The different stabilization of these two orbitals in $Ti_2C_2@D_{3h}$-C_{78} and $Sc_3N@D_{3h}$-C_{78} comes from the position and shape of the metallic cluster. The most stabilized MOs are those having larger contributions of the C atoms near the metallic (positively charged) ions. As can be seen in Figure 5, E′ orbitals have larger contributions closer to the Ti atoms than A_2', and as a consequence, E′ orbitals are more stabilized in the Ti_2C_2 case. But when the Sc_3N moiety is considered, the scenario is the opposite: A_2' orbital lobes are close to the metallic ions (Sc in this case), whereas those of the E′ orbitals are more delocalized. Consequently, the A_2' orbital is more stabilized than the E′ orbitals in $Sc_3N@C_{78}$.

For each bond, the bonding and antibonding character of the A_2' and E′ newly occupied orbitals allows us to understand the observed changes in the bond lengths. Bonds **4**, **7**, **1**, **b**, and **e** (the latter with small lobes) have antibonding contributions from the E′ newly occupied orbitals, and bonds **1** and **b** from the A_2' one. Their occupation when Ti_2C_2, Sc_3N, and Y_3N clusters are encapsulated induces an increase of these bond lengths (see Table 1 and Figure 5). On the other hand, bonds **c**, **f**, and **d** have bonding contributions in these newly occupied orbitals that lead to smaller bond lengths. However, there are two exceptions: first, in the Ti_2C_2 case, bond **f** increases its length due to the strain produced by the Ti_2C_2 moiety; and second, in the Sc_3N and Y_3N clusters, bond **d** gets longer because of the strain produced by Sc and Y metallic ions. In addition, bond **a** enlarges when the Ti_2C_2 moiety is placed inside the C_{78} fullerene cage because of the strain energy induced by the metallic

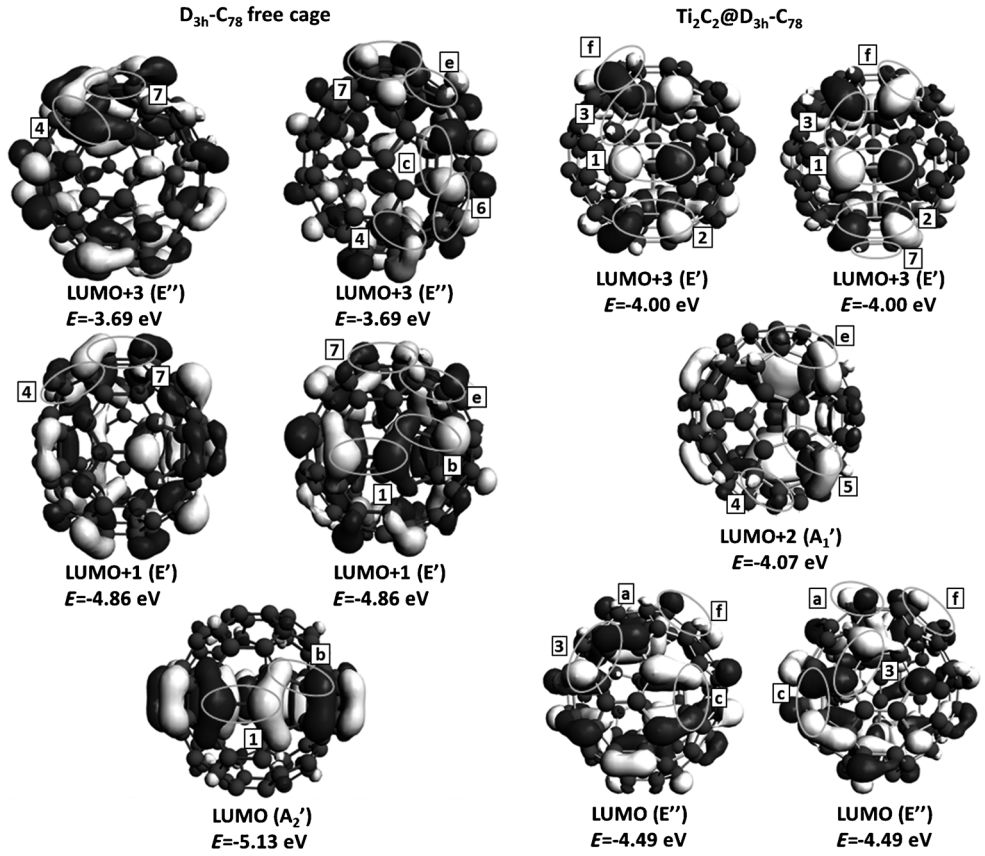

Figure 5. Representation of the D_{3h}-C_{78} free cage LUMO, LUMO+1, and LUMO+3 (isosurface value ±0.02 a.u.) in which only those bonds with favorable orbitals to interact with the HOMO of the diene are marked with ellipses. For comparison the same information is given for Ti_2C_2@ D_{3h}-C_{78}.

cluster. In fact, no antibonding contribution from the newly occupied MO exists to justify this structural change, and, moreover, the length of bond **a** is not modified with respect to that of the C_{78} free cage due to Sc_3N and Y_3N encapsulation. Finally, the length of **2**, **3**, **5**, **6**, and **e** bonds remains more or less unaltered.

The encapsulation of the Ti_2C_2 moiety also induces changes in the rest of the LUMOs. As stated before for the newly occupied orbitals, the LUMOs of the EMFs are stabilized when they have larger contributions close to the metallic ions. As a consequence, the final ordering of the LUMOs depends, at least in part, on the metallic cluster location. In Figure 6, the LUMOs of the Ti_2C_2@C_{78} metallofullerene are represented, and the equivalent for Sc_3N@C_{78} can be found in Figure 8 of reference [14a]. The order of the LUMOs in the Ti_2C_2@C_{78} endofullerene is (in increasing energy order) $E'' < A_1' < E' < E''$, whereas the final order of LUMOs in Sc_3N@C_{78} was $A_1' < A_2'' < E' < E''$. These energy ordering differences can be rationalized by analyzing the position of the metallic cluster inside the fullerene cage. Thus, A_1' and A_2'' LUMOs are more stabilized when the encapsulated moiety is Sc_3N, whereas the E'' orbital is more energetically favored in the presence of the titanium cluster. Finally, the E' LUMO is more or less equally stabilized in the two cases. These differences in the LUMOs imply reactivity changes (see below).

A previous study has shown that the negative charge on the EMF structures is concentrated on the five-membered rings (5-MRs).[31] In the D_{3h}-C_{78} fullerene two nonequivalent 5-MRs (**Y** and **Z**) exist, as can be seen in Figure 2b. In Table 2, we present the Voronoi and Hirshfeld charges of these two nonequivalent 5-MRs for free C_{78}, Sc_3N@C_{78}, Y_3N@C_{78}, and Ti_2C_2@C_{78} fullerenes. 5-MRs that are closer to the metal ions concentrate the largest part of the total negative charge. Thus, 5-MRs **Y** (placed near the Ti atom) have more negative charge in Ti_2C_2@C_{78}, whereas for Sc_3N@C_{78} and Y_3N@C_{78} EMFs the negative charge is mainly located on 5-MRs **Z**. As the total charge transferred from the metallic cluster to the fullerene cage is larger for encapsulated Sc_3N and Y_3N than for Ti_2C_2, 5-MRs in Sc_3N@C_{78} and Y_3N@C_{78} are more negatively charged than those of the Ti_2C_2@C_{78} EMF. The different charge distribution in these systems may be responsible for changes in the reactivity of the C_{78} fullerene cage.

Reaction energies for the Diels–Alder reaction on Ti_2C_2@D_{3h}-C_{78}: The reaction energies obtained at the BP86/TZP//BP86/DZP level for the DA reaction of 1,3-butadiene and all nonequivalent bonds of Ti_2C_2@D_{3h}-C_{78} are listed in Table 3. The reaction energies for free C_{78} are also given for comparison.[14a] All energies are calculated considering 1,3-butadiene in its s-*cis* conformation. For the sake of com-

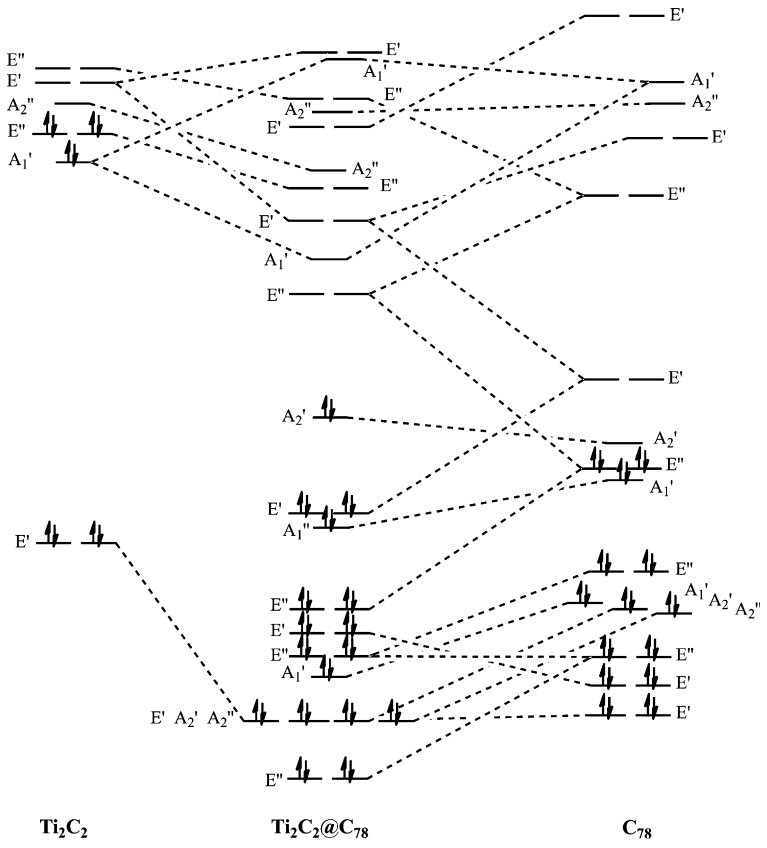

Figure 6. MO-level diagram of the free fullerene, Ti_2C_2, and $Ti_2C_2@D_{3h}$-C_{78}.

Table 2. BP86/TZP//BP86/DZP charges (Hirshfeld and Voronoi, [a.u.]) for the different nonequivalent five-membered rings (5-MRs) in free and endohedral fullerenes. The sum of the charge of the two different 5-MR types and the total 5-MR charges are also presented.

Voronoi	D_{3h}-C_{78}	$Sc_3N@C_{78}$	$Y_3N@C_{78}$	$Ti_2C_2@C_{78}$
Y 5-MRs	−0.016	−0.084	−0.046	−0.136
Z 5-MRs	−0.016	−0.264	−0.254	−0.086
6×**Y** 5-MRs	−0.096	−0.504	−0.276	−0.816
6×**Z** 5-MRs	−0.096	−1.584	−1.524	−0.516
total	−0.192	−2.088	−1.800	−1.332
Hirshfeld	D_{3h}-C_{78}	$Sc_3N@C_{78}$	$Y_3N@C_{78}$	$Ti_2C_2@C_{78}$
Y 5-MRs	−0.032	−0.130	−0.095	−0.143
Z 5-MRs	−0.026	−0.253	−0.268	−0.099
6×**Y** 5-MRs	−0.192	−0.778	−0.572	−0.857
6×**Z** 5-MRs	−0.156	−1.519	−1.605	−0.595
total	−0.348	−2.297	−2.177	−1.452

pleteness, we analyzed the equilibrium between the s-*cis* and s-*trans* conformations with the BP86/TZP//BP86/DZP method. The s-*trans* conformer is 4.0 kcal mol^{-1} more stable than the s-*cis* one and the energy barrier to transform the s-*trans* conformer to the s-*cis* one is 7.7 kcal mol^{-1}. As can be seen in Table 3, in general the reaction is more favored over [5,6] bonds than over [6,6] bonds. Although [6,6] bonds of empty fullerenes are generally more dienophilic (this is not true, however, for C_{78}), DA reactions of EMFs take place preferentially on [5,6] bonds.[2g] Reaction energies are always exothermic for [5,6] type D bonds except for the **b** case, and are endothermic for [6,6] bonds except for the **1** and **3** bonds. This is also reflected in the average values of Table 3. The most favorable addition is produced over the [5,6] bond **c**, for which the reaction energy is −18.1 kcal mol^{-1}, next comes [5,6] bond **f**, with a reaction energy equal to −14.6 kcal mol^{-1}, and [6,6] bond **3** with −14.1 kcal mol^{-1}. In general, there is a reduction of the reaction energies in $Ti_2C_2@D_{3h}$-C_{78} relative to free D_{3h}-C_{78} (average reaction energy values are reduced by 4.2 kcal mol^{-1}, see Table 3). As expected from the smaller electron-donating character of the Ti_2C_2 cluster compared to the Sc_3N one, the reduction in reaction energies, in comparison with C_{78}, is smaller in $Ti_2C_2@D_{3h}$-C_{78} than in $Sc_3N@D_{3h}$-C_{78}. Therefore, our results show that the reactivity is reduced along the series $C_{78} > Ti_2C_2@C_{78} > Sc_3N@C_{78}$.[14a] One could predict the same ordering from the HOMO–LUMO gaps of these species given in the previous section.

Table 3. Reaction energies ΔE_R [kcal mol^{-1}] and bond lengths in the final products of the C−C bonds over which the reaction took place R_{full} [Å], and of the two new C−C bonds formed R_{CC} [Å], for the DA cycloaddition of s-*cis*-1,3-butadiene and $Ti_2C_2@D_{3h}$-C_{78}. Bold values indicate the bonds that are the most reactive under thermodynamic control. For comparison, the E_R values of the free C_{78} fullerene are also given.[a] Average values are calculated taking into account the total number of bonds present in the entire fullerene structure.

		$Ti_2C_2@D_{3h}$-C_{78}				D_{3h}-C_{78}
Product	Bond type	ΔE_R	R_{full}	R_{CC}		ΔE_R[a]
1	A [6,6]	−2.6	1.562	1.575	1.575	**−16.0**
2	C [6,6]	4.2	1.654	1.575	1.575	12.5
3	B [6,6]	**−14.1**	1.625	1.574	1.567	1.8
4	B [6,6]	8.5	1.629	1.571	1.579	−9.2
5	B [6,6]	1.6	1.598	1.576	1.580	0.9
6	B [6,6]	11.1	1.604	1.571	1.591	4.0
7	A [6,6]	5.1	1.667	1.564	1.564	**−18.8**
a	D [5,6]	−7.1	1.728	1.553	1.553	−8.8
b	D [5,6]	3.4	1.623	1.567	1.564	**−23.9**
c	D [5,6]	**−18.1**	1.628	1.562	1.562	−13.3
d	D [5,6]	−6.8	1.616	1.563	1.563	−5.2
e	D [5,6]	−5.5	1.640	1.564	1.566	−13.8
f	D [5,6]	**−14.6**	1.630	1.564	1.548	−5.9
	all bonds	−3.1	1.630	1.568	1.568	−7.3
average	[6,6]	1.2	1.622	1.573	1.576	−2.5
	[5,6]	−7.2	1.637	1.563	1.560	−12.0

[a] Values from ref. [14a].

Interestingly, for $Sc_3N@D_{3h}$-C_{78} the thermodynamically favored bonds were **4**, **6**, and **c**, thus indicating that the orientation of the cluster inside the cage has a large effect on its exohedral reactivity.

Energy barriers for the Diels–Alder reaction on $Ti_2C_2@D_{3h}$-C_{78}: We have also determined the TS structures for the cycloaddition reaction for all nonequivalent bonds of $Ti_2C_2@D_{3h}$-C_{78}. In all cases, the TS search started from a symmetric structure in which the two C–C bonds to be formed have the same length, thus leading in most cases to asynchronous but still concerted TSs. All results are presented in Table 4. For the most asynchronous TSs, that is, bonds **2**, **4**, **6**, and **b**, we checked the possible biradical character of these processes by performing unrestricted UBP86/DZP optimizations in which the TSs were reoptimized and then relaxed in both the forward and backward directions determined by the transition vector (the eigenvector corresponding to the negative eigenvalue) to investigate the possible existence of a biradical intermediate.[32] We found that all TSs were directly connected to reactant and product, thus ruling out the existence of a stepwise mechanism, at least at this level of theory.

Table 4. Reaction barriers $\Delta E^{\neq}$ [kcal mol^{-1}] and bond lengths R_{CC} [Å] for the bonds being formed at the TS in the DA reaction between s-*cis*-1,3-butadiene and $Ti_2C_2@D_{3h}$-C_{78}. Bold values indicate the bonds that are the most reactive under kinetic control. For comparison, the barriers of the free C_{78} fullerene are also given.[a] Average values are calculated taking into account the total number of bonds present in the entire fullerene structure.

Product	Bond type	$Ti_2C_2@D_{3h}$-C_{78} $\Delta E^{\neq}$	R_{CC}		D_{3h}-C_{78} $\Delta E^{\neq}$,[a]
1	A [6,6]	23.6	2.131	2.229	**12.2**
2	C [6,6]	26.8	1.696	2.622	30.2
3	B [6,6]	**18.2**	2.083	2.509	21.7
4	B [6,6]	29.6	1.688	2.397	14.8
5	B [6,6]	20.6	1.843	3.123	14.4
6	B [6,6]	27.0	1.669	2.428	17.2
7	A [6,6]	27.5	1.800	2.490	**13.5**
a	D [5,6]	21.4	2.073	2.219	17.2
b	D [5,6]	26.5	1.678	2.502	**12.5**
c	D [5,6]	**17.4**	2.067	2.562	16.7
d	D [5,6]	22.6	1.850	2.739	22.1
e	D [5,6]	20.5	1.889	3.078	15.3
f	D [5,6]	**19.3**	1.944	2.970	18.0
	all bonds	22.9	1.993	2.540	17.4
average	[6,6]	24.2	1.933	2.506	17.8
	[5,6]	21.7	2.051	2.571	17.0

[a] Values from ref. [14a].

The attack on bond **c** which led to the thermodynamic control product is also the kinetically most favorable among all of the bonds considered (energy barrier of 17.4 kcal mol^{-1}). The other two most exothermic products (**f** and **3**) also have low barriers, but in a different order (18.2 kcal mol^{-1} for bond **3** and 19.3 kcal mol^{-1} for bond **f**).

The other TSs are found at slightly higher energies (20.5–23.6 kcal mol^{-1}) or considerably higher energies (26.5–29.6 kcal mol^{-1}). In general, there is a good but not exact correlation between the thermodynamic and kinetic ordering of reactivity. The highest barrier is found for bond **4**, which has the second most endothermic reaction energy value. Bond **6**, with the most endothermic reaction energy, also has a large reaction barrier (27.0 kcal mol^{-1}).

Therefore, the cycloaddition reaction over [5,6] bonds is usually favored with respect to [6,6], not only from a thermodynamic point of view, but also from a kinetic one (on average, [5,6] barriers are 2.5 kcal mol^{-1} lower than [6,6] ones). However, there are several exceptions, such as bond **b** (type D, [5,6]), which has an endothermic reaction energy and a high reaction barrier, or bond **3**, as we said, one of the three most reactive bonds. From a kinetic point of view, it is also found that free D_{3h}-C_{78} is the most reactive cage followed by $Ti_2C_2@D_{3h}$-C_{78}, which is in turn more reactive than $Sc_3N@D_{3h}$-C_{78}.[14a]

Rationalization of the $Ti_2C_2@D_{3h}$-C_{78} reactivity: Bond lengths, pyramidalization angles, atomic charges, MOs, deformation energies, and noncluster energy barriers: It is usually found in fullerenes that cycloadditions occur preferentially on short C–C bonds, with high pyramidalization angles, and having lobes on each C atom of opposite sign in some of the LUMOs of the fullerene to facilitate the interaction with the HOMO of the diene. Let us now analyze these aspects for the particular case of the DA cycloaddition to $Ti_2C_2@D_{3h}$-C_{78}.

The principal changes in the fullerene structure induced by the encapsulation of a Ti_2C_2 metallic cluster are found in the bonds close to the titanium ions. Thus, bond **7** (type A, [6,6]) and bond **a** (type D, [5,6]) increase their lengths significantly with respect to the free cage. As we said before, the increase in the length of bond **7** is also the result of charge transfer from the metallic cluster to the cage. As can be seen in Tables 3 and 4, this bond length enlargement plays against their reactivity. Furthermore, their pyramidalization angles also increase considerably, but this is not sufficient to make them more reactive. On the other hand, the C–C separations of bonds **1**, **4**, and **b** also increases (see below) and these bonds become less reactive.

The most reactive bonds, **c** (type D, [5,6]), **f** (type D, [5,6]), and **3** (type B, [6,6]), are slightly favored by the inclusion of the titanium cluster inside the C_{78}. The bond length reduction in bonds **c** and **3** justify in part their higher reactivity as compared to free C_{78}. In the case of bond **c**, in addition, the pyramidalization angle is somewhat higher, thus favoring its reactivity. Bond **f** remains more or less the same with a small increase in the bond length. However, its reactivity is clearly increased, being one of the most reactive bonds for $Ti_2C_2@D_{3h}$-C_{78}. This is mainly attributed to electronic (not structural) effects due to the presence of the metallic cluster inside the fullerene cage (see below). All the remaining bonds are hardly modified by the inclusion of the metallic carbide, having similar structural parameters with respect to the C_{78} free cage. It is worth noting that neither bond **1**, with the shortest C–C bond length, nor bonds **7**

and **a**, with the highest pyramidalization angles, are among the most reactive bonds. As found in previous studies, reactivity predictions made from bond lengths and pyramidalization angles show many inconsistencies.[14]

It can be seen in Figure 4 that for the $Ti_2C_2@D_{3h}$-C_{78} compound the most favorable bonds under thermodynamic and kinetic conditions (bonds **c**, **3**, and **f**) present favorable LUMOs (degenerate) to interact with the HOMO of the diene. The LUMOs also present an adequate shape for the DA reaction on bond **a**. In the LUMO+2 orbital, bonds **e**, **4**, and **5** have the correct lobe shape for the reaction with the diene. In fact, bonds **e** and **5** have only slightly larger reaction barriers than **c**, **3**, and **f** bonds. In contrast, bond **4** has the largest energy barrier of all nonequivalent bonds. Finally, the shape of the LUMO+3 degenerate orbitals is favorable for the interaction of butadiene with bonds **1**, **2**, **3**, **f**, and **7**. Bonds **1**, **2**, and **7** have higher reaction barriers than bonds having correctly oriented lobes in the LUMO+2 and LUMO. Bonds **3** and **f** have smaller barriers, but they can interact through the LUMO. Therefore, we can conclude that the most reactive bonds present LUMOs with a suitable shape to interact with the HOMO of the diene during the cycloaddition reaction. We have also found that, in general, for a given bond, the lower the energy of the LUMO with an appropriate contribution from the bond to interact favorably with the diene, the higher its reactivity. As a whole, we find that having LUMOs with the proper shape for the interaction is a good but not sufficient condition for a given bond to be reactive. Thus, from this MO analysis, one could predict that bond **4** must have an energy barrier similar to those of bonds **5** and **e**, but it has the highest one. Bond **a** should be also predicted as quite reactive, but it is not. Another important observation to take into account is that bond **d**, which is quite reactive, is not present in any of the LUMOs analyzed. Therefore, the MO analysis affords interesting conclusions but as a predictive tool it also shows many inconsistencies. However, the combination of the three parameters (short bond lengths, high pyramidalization angles, and appropriate shape of the LUMOs) provides a good criterion for predictions on the chemical reactivity of the different bonds, as seen in a previous study.[14a]

We found that [6,6] bonds in $Ti_2C_2@D_{3h}$-C_{78} that are placed next to the most charged 5-MRs **Y** (bonds **4**, **6**, and **7**) are those with the lowest reactivity. That is, they have been deactivated. On the other hand, [6,6] bonds placed next to the **Z** 5-MRs (**1**, **3**, and **5**), which have a lower negative charge, are the most reactive [6,6] bonds and one of them, bond **3**, is one of the most reactive bonds of the system. This behavior could be ascribed to the electronic requirements for the DA reaction. DA cycloadditions are favored for dienes rich in electrons and electron-poor dienophiles (otherwise an inverse-demand DA is produced). The [6,6] bonds placed next to 5-MRs that concentrate more negative charge are more electron rich and, therefore, their DA reactivity is expected to be lower.

The TS deformation energy (also called TS distortion energy[33] and activation strain energy[34]) of the fullerene is defined as the energy required to distort the cage of the fullerene from its optimized geometry to the geometry it has in the TS. It has been found that there is a good relationship between this deformation energy and the energy barrier for some cycloaddition reactions.[33,35] Herein, we propose a new concept, the noncluster energy barrier, which is defined as the energy difference between the TS and reactants when the Ti_2C_2 cluster is removed from the EMF, while keeping the geometry of the reactants and TS frozen. The noncluster energy barrier gives an idea of the geometric effect of the cluster on the energy barrier. The difference between the actual energy barrier and the noncluster energy barrier is an indication of the purely electronic effect of the Ti_2C_2 cluster on the energy barrier. If this difference is negative, it means that the electron transfer from the Ti_2C_2 cluster favors this addition, and vice versa. Bonds that have low energy differences are those in which the charge transfer from the Ti_2C_2 cluster does not have a large effect on their final reactivity. However, one has to admit here that the geometry changes in the cage are at least in part due to electronic effects (charge transfer from the Ti_2C_2 to the LUMOs of the C_{78} cage results in geometric changes, see above), so it is not possible to exactly separate the two effects. In spite of this, the results obtained for the noncluster energy barriers are quite informative.

Although neither the deformation energies at the TS nor the noncluster energy barriers have predictive value, they are worth analyzing to understand the reactivity trends. Table 5 lists the fullerene deformation energy at the TS, the noncluster energy barriers, and the difference between actual energy barriers and noncluster energy barriers for all nonequivalent bonds of the DA reaction between $Ti_2C_2@D_{3h}$-C_{78} and s-*cis*-1,3-butadiene. Deformation energies

Table 5. Fullerene deformation energy at the transition state $\Delta E^{\ddagger}_{\text{def. ful.}}$ [kcal mol^{-1}], noncluster energy barriers $\Delta E^{\ddagger}_{\text{no\_Ti}_2\text{C}_2}$ [kcal mol^{-1}], and the difference between actual energy barriers (Table 4) and noncluster energy barriers $\Delta E^{\ddagger}-\Delta E^{\ddagger}_{\text{no\_Ti}_2\text{C}_2}$ [kcal mol^{-1}] for all nonequivalent bonds of the $Ti_2C_2@D_{3h}$-C_{78} DA reaction. Average values are calculated taking into account the total number of bonds present in the entire fullerene structure.

		$Ti_2C_2@D_{3h}$-C_{78}		
Product	Bond type	$\Delta E^{\ddagger}_{\text{def. ful.}}$	$\Delta E^{\ddagger}_{\text{no\_Ti}_2\text{C}_2}$	$\Delta E^{\ddagger}-\Delta E^{\ddagger}_{\text{no\_Ti}_2\text{C}_2}$
1	A [6,6]	9.2	6.8	16.8
2	C [6,6]	19.6	25.6	1.2
3	B [6,6]	8.8	17.4	0.8
4	B [6,6]	20.3	6.8	22.8
5	B [6,6]	10.6	8.1	12.5
6	B [6,6]	23.7	21.5	5.5
7	A [6,6]	15.6	3.5	24.0
a	D [5,6]	9.0	11.0	10.4
b	D [5,6]	17.8	−1.2	27.7
c	D [5,6]	7.2	14.1	3.3
d	D [5,6]	11.8	11.7	10.9
e	D [5,6]	12.7	7.7	12.8
f	D [5,6]	12.2	25.2	−5.9
	all bonds	13.7	11.8	11.1
average	[6,6]	15.0	12.5	11.8
	[5,6]	12.5	11.2	10.5

of the diene, for which we observed a general correlation with the fullerene deformation energies, are given in Table S1 of the Supporting Information. It was found that, in general, the larger the fullerene deformation energies, the larger the diene deformation energy. First, we will focus on the fullerene deformation energies ($\Delta E^{\neq}_{\text{def. ful.}}$). Bonds which present lower fullerene deformation energies (from 7.2 to 12.7 kcal mol^{-1}) are **1**, **3**, **5**, **a**, **c**, **d**, **e**, and **f**. The other nonequivalent bonds (**2**, **4**, **6,** **7**, and **b**) present fullerene deformation energies between 15.6 and 23.7 kcal mol^{-1}. These latter bonds are those having in the TS a forming C–C bond length shorter than 1.8 Å and high asynchronicity. In these bonds, the diene and dienophile have to approach at short distance to get good $HOMO_{diene}$–$LUMO_{dienophile}$ interactions and, consequently, the TS is found later in the reaction coordinate and the deformation is higher. Here, it is important to remark that the two least reactive bonds (thermodynamically and kinetically), **4** and **6**, are those which have the highest fullerene deformation energies. Their poor reactivity is translated into a large energy required to distort the fullerene cage to the geometry it has in the TS when reaction takes place over one of these two bonds. There is not, however, an exact correspondence between deformation energies at the TS and energy barriers. For instance, bond **1** has low deformation energy and a relatively high energy barrier. Similarly, bond **6** with the largest deformation energy does not possess the highest barrier.

Bonds that have low differences in actual energy barriers and noncluster energy barriers are those in which the orbital interactions between the Ti_2C_2 cluster and the cage (including charge transfer from the cluster) do not have a large effect on their final reactivity (Table 5). These bonds are **2**, **3**, **6**, **c**, and **f**, with energy differences between −5.9 and 5.5 kcal mol^{-1}. For the other nonequivalent bonds (**1**, **4**, **5**, **7**, **a**, **b**, **d**, and **e**), the presence of the metallic cluster implies an increase of the reaction barrier with values going from 10.4 to 27.7 kcal mol^{-1} and, therefore, a reduction of reactivity that has to be attributed to orbital interactions (charge transfer + polarization) with the metallic cluster. Indeed for all bonds, except **f**, there is a reduction of reactivity due to orbital interactions of the cage with the Ti_2C_2 unit. For bond **f** the energy barrier difference is negative (−5.9 kcal mol^{-1}) and this means that the reactivity of bond **f** is enhanced because of charge transfer and polarization from the Ti_2C_2 moiety. If we look at the MOs of the free C_{78} cage in Figure 4, it can be seen that the LUMOs do not have the right shape for a good interaction with bond **f**. On the other hand, the LUMOs (LUMO E″ and LUMO+3 E′) of $Ti_2C_2@C_{78}$ have contributions from bond **f** with lobes having the required opposite signs on each C atom. It is worth noting that the presence of the titanium cluster stabilizes these E″ and E′ orbitals with respect to free C_{78}. Thus, orbital interactions of the cage with the Ti_2C_2 cluster change the LUMOs and make them more suitable for the DA reaction with bond **f**.

An additional important observation is that there are only three bonds (**c**, **f**, and **3**) that have low fullerene deformation energies and low differences between reaction barriers and noncluster energy barriers. As we have explained before, these three bonds are the ones with the lowest energy barriers and highest exothermicity. On the other hand, there are only three bonds (**4**, **7**, and **b**) that are disfavored by these two parameters and they are among the bonds with the highest energy barriers and endothermicities.

As a whole, compared to free C_{78}, for $Ti_2C_2@D_{3h}$-C_{78} we find:

1) Bond **1** is quite reactive in free C_{78} and its reactivity is clearly reduced in $Ti_2C_2@D_{3h}$-C_{78}. The reason is not structural (bond length and pyramidalization angles are similar) but electronic (occupancy of C_{78} LUMOs A_2' and E″, which have the correct energy and shape) as derived from the noncluster energy barriers.
2) Bond **2** is quite unreactive for all systems because of its large C–C bond length and low pyramidalization angles (it is actually the unreactive pyrene or type C bond).
3) Bond **3**, in free C_{78}, is not especially reactive. With the inclusion of the Ti_2C_2 cluster it becomes much more reactive. The charge transfer from the cluster reduces its C–C bond length, whereas the strain slightly increases the pyramidalization angles. Purely electronic effects are close to zero for this bond.
4) Bond **4** is not particularly reactive in free C_{78} and it is clearly deactivated in $Ti_2C_2@D_{3h}$-C_{78}. This is due in part to structural effects (bond length increases and pyramidalization angles are reduced) and also to electronic effects.
5) Bond **5**'s reactivity is reduced in $Ti_2C_2@D_{3h}$-C_{78} due to electronic effects.
6) Bond **6** is reactive neither in free C_{78} nor in $Ti_2C_2@D_{3h}$-C_{78}. No LUMOs are available with the correct lobes for the DA addition.
7) Bond **7**, in free C_{78}, is one of the most reactive bonds, but when a metallic cluster is encapsulated its reactivity decreases rapidly. For $Ti_2C_2@D_{3h}$-C_{78}, it becomes one of the least reactive bonds because of electronic effects, similar to what happens with bond **1**.
8) Bond **a** is quite unreactive for all systems because of the large C–C bond length.
9) Bond **b**, for free C_{78}, is a very reactive [5,6] bond. It is the [5,6] bond with the shortest C–C bond length. Encapsulation of Ti_2C_2 dramatically reduces its reactivity due to both structural (longer C–C bond length) and electronic effects.
10) Bond **c**, in free C_{78}, is quite reactive. In $Ti_2C_2@D_{3h}$-C_{78}, this bond is shortened and has a similar reactivity to that for free C_{78}. It is the [5,6] bond in this EMF with the shortest C–C bond length. In addition, the electronic effects of encapsulation on this bond are one of the smallest for the series.
11) Bond **d**, with a relatively larger C–C bond length, is unreactive in both free C_{78} and $Ti_2C_2@D_{3h}$-C_{78}. It becomes reactive in $Y_3N@D_{3h}$-C_{78} because of strain.[14b]

12) Bond **e** is not very reactive in free C_{78} and is clearly deactivated in $Ti_2C_2@D_{3h}$-C_{78}. This is not due to structural effects (bond length decreases and pyramidalization angle increases), but to electronic effects.
13) Bond **f** is not reactive in free C_{78} and becomes one of the most reactive in $Ti_2C_2@D_{3h}$-C_{78} due to electronic effects. It is the only bond favored (energy barriers are reduced) by the charge transfer and polarization from the metallic cluster.

Effect of the cluster nature and fullerene strain on the exohedral reactivity of D_{3h}-C_{78} endofullerene compounds: the reactivity of $Ti_2C_2@D_{3h}$-C_{78} and $M_3N@D_{3h}$-C_{78} (M=Sc and Y) EMFs: In two previous papers,[14] we have compared the reactivity of free D_{3h}-C_{78} and encapsulated TNT EMFs $M_3N@D_{3h}$-C_{78} (M=Sc and Y). Our results indicated that in general there is a reduction in exohedral reactivity on going from D_{3h}-C_{78} to $Sc_3N@D_{3h}$-C_{78}. In turn, the reactivity of most bonds (for instance bonds **5**, **7**, **b**, **c**, and **e**) decreases slightly when changing scandium for yttrium in $Sc_3N@D_{3h}$-C_{78}. This reduction of reactivity was attributed to the slightly larger electron transfer from the Y_3N unit to the fullerene, which pushes the LUMOs up and leads to a somewhat higher HOMO–LUMO energy gap in $Y_3N@D_{3h}$-C_{78} than in $Sc_3N@D_{3h}$-C_{78} (1.26 vs. 1.22 eV). For some bonds (especially bond **d** but also **1** and **3**), however, the reactivity is enhanced in $Y_3N@D_{3h}$-C_{78}. This was caused by the larger strain in these bonds induced by the bigger Y_3N TNT unit. In this work, we analyzed the DA reaction on the $Ti_2C_2@D_{3h}$-C_{78} species. As the same isomer is considered (D_{3h}) in all the different studies that have been carried out using the same method of calculation, any differences in reactivity can be directly attributed to the electronic effects of the metallic cluster encapsulated inside the cage and the strain energy it causes. So, we now compare the results obtained for the $Ti_2C_2@D_{3h}$-C_{78} EMF with the previously studied systems.

Figures 7 and 8 compare the reaction energies and energy barriers for all bonds of the species analyzed. Between $Ti_2C_2@C_{78}$ and the previously studied systems, there exist many differences in reactivity, mainly caused by the different orientation of the metallic cluster inside the fullerene cage. The effect of the Ti_2C_2 cluster leads in general to a decrease in reactivity as compared to the free C_{78}. This is the same effect (but somewhat less severe) as that produced by the Sc_3N unit. In both clusters we have similar deformation energies due to encapsulation (not especially high indicating relatively low fullerene cage strain) and similar changes in

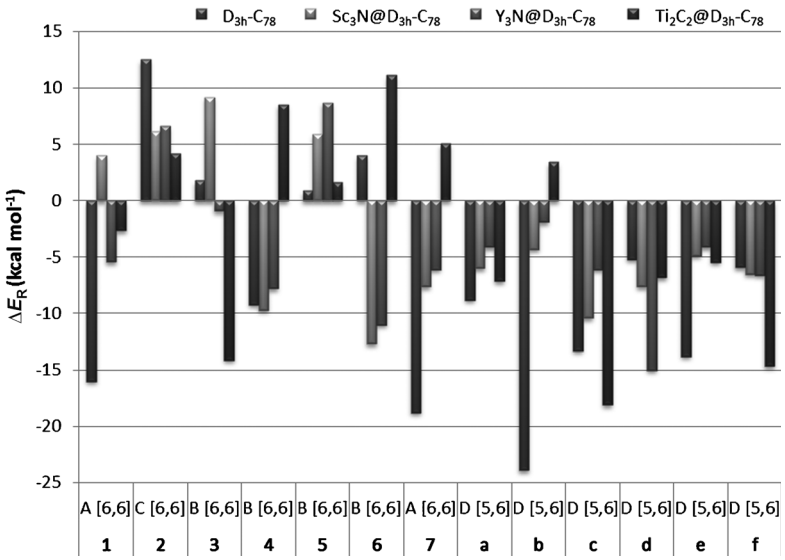

Figure 7. Comparison of the reaction energies [kcal mol^{-1}] found for the DA reaction of s-*cis*-1,3-butadiene over the nonequivalent bonds of the free D_{3h}-C_{78} cage (dark gray),[14a] $Sc_3N@D_{3h}$-C_{78} (light gray),[14a] $Y_3N@D_{3h}$-C_{78} (gray),[14b] and $Ti_2C_2@D_{3h}$-C_{78} (black). Only results for the down region of $Y_3N@D_{3h}$-C_{78} are reported here.

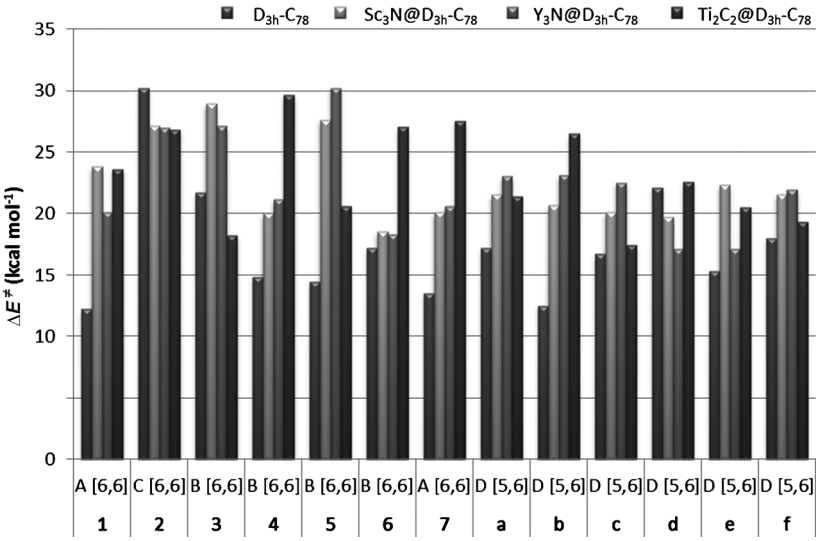

Figure 8. Comparison of the energy barriers [kcal mol^{-1}] found for the DA reaction of s-*cis*-1,3-butadiene over the nonequivalent bonds of the free D_{3h}-C_{78} cage (dark gray),[14a] $Sc_3N@D_{3h}$-C_{78} (light gray),[14a] $Y_3N@D_{3h}$-C_{78} (gray),[14b] and $Ti_2C_2@D_{3h}$-C_{78} (black). Only results for the down region of $Y_3N@D_{3h}$-C_{78} are reported here.

reactivity, the most favored bonds being short [5,6] bonds close to the metals and [6,6] bonds far from the cluster. The favored bonds, however, differ. Thus, compared to $Sc_3N@D_{3h}$-C_{78} EMF, the Ti_2C_2 cluster clearly decreases the reactivity of the **4**, **6**, **7**, and **b** bonds, whereas it makes bonds **3**, **c**, and **f** more reactive. On the other hand, the Sc_3N cluster favors the reactivity of the **6** and **d** bonds. The change in reactivity is due to the different ordering of the LUMOs of the C_{78} fullerene cage with the correct energy and shape for the reaction to proceed, and which have been modified because of the orbital interactions with the metal cluster (see above). Thus, the E″ LUMOs of $Ti_2C_2@D_{3h}$-C_{78} have an important and suitable contribution from bonds **3**, **c**, and **f**.

During this study, we found that [6,6] bonds which are placed next to 5-MRs that have the greatest charge are deactivated. In the Sc_3N and Y_3N cases, the most charged rings are type **Z** 5-MRs instead of type **Y**, which are the most charged in the Ti_2C_2 system. As can be seen in Figures 7 and 8, the most reactive [6,6] bonds in scandium and yttrium systems are bonds **7**, **4**, and **6**, all of them placed next to type **Y** rings. Again, [6,6] bonds next to 5-MRs with lower charge are the most favored, instead of those which are placed near highly charged 5-MRs (type **Z**) that are deactivated by electronic effects.

An exceptional case is bond **2**, the only pyrenic type C bond that has no 5-MR placed next to it, and the reactivity of which remains constant for all three EMFs studied in this and previous studies. This shows that the effect of the electronic charge of 5-MRs is very important to understand the [6,6] bond reactivity in metallofullerenes.

Changes in the energy profile due to dispersion corrections: In a recent study, we have shown that dispersion corrections are essential for the investigation of the chemical reactivity of fullerenes and nanotubes.[29] Herein, we include them at the end of our study because our main goal was to compare the changes in chemical reactivity due to the different encapsulated metallic clusters, and previous studies were performed without dispersion corrections. Now, we explore the effect of including dispersion corrections on the potential energy surface of this DA reaction. The numerical results are gathered in Table 6, and Figure 9 compares the two profiles obtained with and without dispersion corrections for the most reactive [6,6] bond.

The results in Table 6 show that the inclusion of dispersion corrections leads in general to an increase of the exothermicity of the DA reactions by 11.2–13.5 kcal mol^{-1} (average 12.6 kcal mol^{-1}). Likewise, reaction barriers decrease by about 11.2–13.5 kcal mol^{-1} (average 12.3 kcal mol^{-1}) after inclusion of dispersion effects. Moreover, with dispersion corrections included, we find an initial complex formed by London dispersion interactions that causes a stabilization of reactants of about 1.3–3.6 kcal mol^{-1} (average 3.1 kcal mol^{-1}). All these changes are relevant. However, if we order all nonequivalent bonds according to their reactivity with or without including dispersion effects, we can see that although the numbers change due to dispersion effects, the observed trends are the same. Therefore, although dispersion energy corrections are essential to correctly reproduce the thermodynamics and kinetics of the DA reaction, the reactivity trends remain unchanged. Hence, we have shown convincingly that the conclusions drawn from our reactivity comparison study performed without including dispersion corrections will remain the same with the inclusion of dispersion corrections.

Table 6. Reaction energies ΔE_R [kcal mol^{-1}] and reaction barriers $\Delta E^{\neq}$ [kcal mol^{-1}] with and without energy dispersion corrections (D_3), and reaction energies and barriers using as a reference the reactant complex formed, $\Delta E_{R\,int}$, $\Delta E^{\neq}_{int}$ [kcal mol^{-1}].

		$Ti_2C_2@D_{3h}$-C_{78}					
Product	Bond type	ΔE_R	ΔE_R (D_3)	$\Delta E_{R\,int}$ (D_3)	$\Delta E^{\neq}$	$\Delta E^{\neq}$ (D_3)	$\Delta E^{\neq}_{int}$ (D_3)
1	A [6,6]	−2.6	−13.8	−12.6	23.6	10.9	12.1
2	C [6,6]	4.2	−8.6	−6.4	26.8	14.3	16.4
3	B [6,6]	−14.1	−26.8	−23.6	18.3	5.4	8.6
4	B [6,6]	8.5	−4.2	−0.8	29.7	16.4	19.8
5	B [6,6]	1.6	−10.8	−8.2	20.6	9.4	12.0
6	B [6,6]	11.1	−1.5	2.2	27.0	13.5	17.2
7	A [6,6]	5.1	−7.8	−5.6	27.5	15.7	17.9
a	D [5,6]	−7.1	−19.6	−16.9	21.4	9.1	11.8
b	D [5,6]	3.4	−8.9	−6.4	26.5	14.2	16.7
c	D [5,6]	−18.1	−29.3	−27.2	17.4	5.1	7.2
d	D [5,6]	−6.8	−19.0	−16.2	22.6	10.6	13.4
e	D [5,6]	−5.5	−19.0	−16.0	20.5	8.2	11.2
f	D [5,6]	−14.6	−28.0	−24.8	19.3	7.3	10.5
	all bonds	−3.1	−15.7	−12.9	22.9	10.6	13.4
average	[6,6]	1.2	−11.4	−8.5	24.2	11.7	14.5
	[5,6]	−7.2	−19.9	−17.1	21.7	9.5	12.3

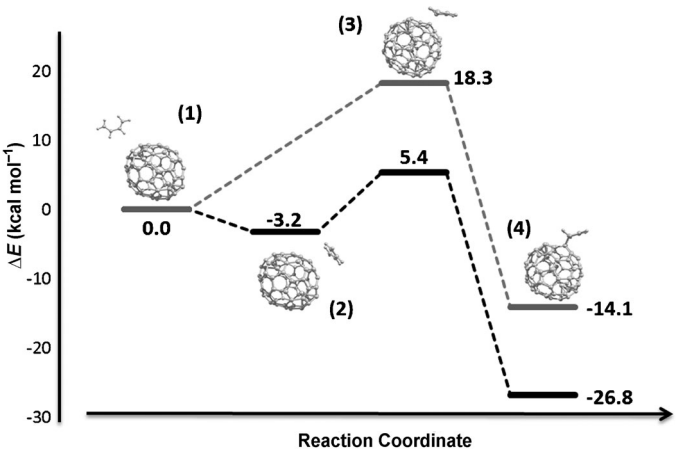

Figure 9. Energy profile of the DA cycloaddition between $Ti_2C_2@D_{3h}$-C_{78} and s-*cis*-1,3-butadiene obtained when including dispersion effects (black) and when they were not taken into account (gray) for the attack over the most reactive [6,6] bond (bond **3**). The stationary points represented are: 1) reactants; 2) reactant complex structure; 3) transition state; and 4) product. Relative energy values are given in kcal mol^{-1}.

Conclusion

We have analyzed the DA reaction of 1,3-butadiene with all nonequivalent bonds of $Ti_2C_2@D_{3h}$-C_{78}. Our results showed that the regioselectivity of this exohedral addition is extremely modified by changing the nature of the cluster encapsulated inside, and is different from those obtained in previous studies on M_3N-encapsulated D_{3h}-C_{78}. The preference for reacting with a given bond is due to different factors: first, charge transfer from the metallic cluster to the cage that changes certain C–C bond lengths; second, fullerene deformation caused by the presence of a metallic cluster inside, which has an important influence on the C–C bond lengths and their reactivity; and third, changes in LUMOs of the fullerene cage induced by the metallic cluster that determine the final predisposition of different bonds to interact with the HOMO of the diene.

We find that, as compared to free C_{78} for which [6,6] **1** and **6** bonds and the [5,6] **b** bond are the preferred addition sites, the Ti_2C_2 cluster favors addition to the [6,6] **3** bond and the [5,6] **c** and **f** bonds. Moreover, in general, the reactivity decreases when going from free D_{3h}-C_{78} to $Ti_2C_2@D_{3h}$-C_{78}. Ti_2C_2 and Sc_3N clusters have similar encapsulation energies and similar changes in reactivity, the most favored bonds being [5,6] bonds close to the metals and [6,6] bonds far from the cluster. However, the Sc_3N cluster favors the reactivity of the **6** and **d** bonds, whereas the **3**, **c**, and **f** addition sites are the preferred ones in $Ti_2C_2@D_{3h}$-C_{78}. Interestingly, we have found that [6,6] bonds closer to the most charged 5-MR in the cage are deactivated.

Finally, we have studied the inclusion of dispersion corrections for this cycloaddition reaction. Only when dispersion corrections are taken into account do we find an initial reactant complex with a stabilization relative to reactants of about 1–3 kcal mol^{-1}. Moreover, the dispersion corrections lead to changes in barriers and reaction energies of about 12 kcal mol^{-1}. Although including dispersion corrections changes reaction barriers and reaction energies, the reactivity trends remain the same. Therefore, the study of the regioselectivity of a reaction does not depend on the inclusion of the dispersion corrections.

Acknowledgements

The following organizations are thanked for financial support: the Spanish Ministerio de Ciencia e Innovación (MICINN, project numbers CTQ2008-03077/BQU, CTQ2008-06532/BQU, and CTQ2011-23156/BQU), and the DIUE of the Generalitat de Catalunya (project numbers 2009SGR637 and 2009SGR528). Financial support from MICINN and the FEDER fund (European Fund for Regional Development) was provided by grant UNGI08-4E-003. M.G.-B. thanks the Spanish Ministerio de Educación, Cultura y Deporte for the doctoral fellowship number AP2010-2517. S.O. is grateful to the European Community for postdoctoral fellowship PIOF-GA-2009-252856. Excellent service by the Centre de Serveis Científics i Acadèmics de Catalunya (CESCA) is gratefully acknowledged. The authors are also grateful for the computer resources, technical expertise, and assistance provided by the Barcelona Supercomputing Center—Centro Nacional de Supercomputación. Support for the research of M. Solà was received through the ICREA Academia 2009 prize for excellence in research funded by the DIUE of the Generalitat de Catalunya.

[1] J. R. Heath, S. C. O'Brien, Q. Zhang, Y. Liu, R. F. Curl, H. W. Kroto, F. K. Tittel, R. E. Smalley, *J. Am. Chem. Soc.* **1985**, *107*, 7779.
[2] a) S. Liu, S. Sun, *J. Organomet. Chem.* **2000**, *599*, 74; b) S. Guha, K. Nakamoto, *Coord. Chem. Rev.* **2005**, *249*, 1111; c) M. Murata, Y. Murata, K. Komatsu, *Chem. Commun.* **2008**, 6083; d) M. N. Chaur, F. Melin, A. L. Ortiz, L. Echegoyen, *Angew. Chem.* **2009**, *121*, 7650; *Angew. Chem. Int. Ed.* **2009**, *48*, 7514; e) M. Yamada, T. Akasaka, S. Nagase, *Acc. Chem. Res.* **2010**, *43*, 92; f) A. Rodríguez-Fortea, A. L. Balch, J. M. Poblet, *Chem. Soc. Rev.* **2011**, *40*, 3551; g) X. Lu, T. Akasaka, S. Nagase, *Chem. Commun.* **2011**, *47*, 5942.
[3] C.-R. Wang, T. Kai, T. Tomiyama, T. Yoshida, Y. Kobayashi, E. Nishibori, M. Takata, M. Sakata, H. Shinohara, *Angew. Chem.* **2001**, *113*, 411; *Angew. Chem. Int. Ed.* **2001**, *40*, 397.
[4] C.-R. Wang, M. Inakuma, H. Shinohara, *Chem. Phys. Lett.* **1999**, *300*, 379.
[5] a) Y. Iiduka, T. Wakahara, K. Nakajima, T. Tsuchiya, T. Nakahodo, Y. Maeda, T. Akasaka, N. Mizorogi, S. Nagase, *Chem. Commun.* **2006**, 2057; b) Y. Iiduka, T. Wakahara, T. Nakahodo, T. Tsuchiya, A. Sakuraba, Y. Maeda, T. Akasaka, K. Yoza, E. Horn, T. Kato, M. T. H. Liu, N. Mizorogi, K. Kobayashi, S. Nagase, *J. Am. Chem. Soc.* **2005**, *127*, 12500; c) E. Nishibori, S. Narioka, M. Takata, M. Sakata, T. Inoue, H. Shinohara, *ChemPhysChem* **2006**, *7*, 345; d) T. Inoue, T. Tomiyama, T. Sugai, H. Shinohara, *Chem. Phys. Lett.* **2003**, *382*, 226; e) T. Inoue, T. Tomiyama, T. Sugai, T. Okazaki, T. Suematsu, N. Fujii, H. Utsumi, K. Nojima, H. Shinohara, *J. Phys. Chem. B* **2004**, *108*, 7573.
[6] A. A. Popov, L. Zhang, L. Dunsch, *ACS Nano* **2010**, *4*, 795.
[7] a) B. Cao, M. Hasegawa, K. Okada, T. Tomiyama, T. Okasaki, K. Suenaga, H. Shinohara, *J. Am. Chem. Soc.* **2001**, *123*, 9679; b) R. Jaffiol, A. Débarre, C. Julien, D. Nutarelli, P. Tchénio, A. Taninaka, B. Cao, T. Okasaki, H. Shinohara, *Phys. Rev. B* **2003**, *68*, 014105; c) K. Iwasaki, S. Hino, D. Yoshimura, B. Cao, T. Okasaki, H. Shinohara, *Chem. Phys. Lett.* **2004**, *397*, 169; d) K. Tan, X. Lu, *Chem. Commun.* **2005**, 4444; e) T. Yumura, Y. Sato, K. Suenaga, S. Iijima, *J. Phys. Chem. B* **2005**, *109*, 20251.
[8] Z.-Q. Shi, X. Wu, C.-R. Wang, X. Lu, H. Shinohara, *Angew. Chem.* **2006**, *118*, 2161; *Angew. Chem. Int. Ed.* **2006**, *45*, 2107.
[9] R. Valencia, A. Rodríguez-Fortea, J. M. Poblet, *J. Phys. Chem. A* **2008**, *112*, 4550.
[10] Y. Iiduka, T. Wakahara, K. Nakajima, T. Nakahodo, T. Tsuchiya, Y. Maeda, T. Akasaka, K. Yoza, M. T. H. Liu, N. Mizorogi, S. Nagase, *Angew. Chem.* **2007**, *119*, 5658; *Angew. Chem. Int. Ed.* **2007**, *46*, 5562.
[11] T. Akasaka, S. Nagase, K. Kobayashi, T. Suzuki, T. Kato, K. Kikuchi, Y. Achiba, K. Yamamoto, H. Funasaka, T. Takahashi, *Angew. Chem.* **1995**, *107*, 2303; *Angew. Chem. Int. Ed. Engl.* **1995**, *34*, 2139.
[12] T. Wang, J. Wu, W. Xu, J. Xiang, X. Lu, B. Li, L. Jiang, C. Shu, C. Wang, *Angew. Chem.* **2010**, *122*, 1830; *Angew. Chem. Int. Ed.* **2010**, *49*, 1786.
[13] S. Osuna, M. Swart, M. Solà, *Phys. Chem. Chem. Phys.* **2011**, *13*, 3585.
[14] a) S. Osuna, M. Swart, J. M. Campanera, J. M. Poblet, M. Solà, *J. Am. Chem. Soc.* **2008**, *130*, 6206; b) S. Osuna, M. Swart, M. Solà, *J. Am. Chem. Soc.* **2009**, *131*, 129.
[15] a) G. te Velde, F. M. Bickelhaupt, E. J. Baerends, C. Fonseca Guerra, S. J. A. van Gisbergen, J. G. Snijders, T. Ziegler, *J. Comput. Chem.* **2001**, *22*, 931; b) ADF2010.01, E. J. Baerends, T. Ziegler J. Autschbach, D. Bashford, J. A. Berger, A. Bérces, F. M. Bickelhaupt, C. Bo, P. L. de Boeij, P. M. Boerrigter, L. Cavallo, D. P. Chong, L. Deng, R. M. Dickson, D. E. Ellis, M. van Faassen, L. Fan, T. H. Fischer, A. Giammona, A. Ghysels, C. Fonseca Guerra, S. J. A. van Gisbergen, A. W. Götz, J. A. Groeneveld, O. V. Gritsenko, M. Grüning, S. Gusarov, F. E. Harris, P. van den Hoek, C. R. Jacob, H. Jacobsen, L. Jensen, E. S. Kadantsev, J. K. Kaminski, G. van Kessel, R.

Klooster, F. Kootstra, A. Kovalenko, M. V. Krykunov, E. van Lenthe, J. N. Louwen, D. A. McCormack, A. Michalak, M. Mitoraj, J. Neugebauer, V. P. Nicu, L. Noodleman, V. P. Osinga, S. Patchkovskii, P. H. T. Philipsen, D. Post, C. C. Pye, W. Ravenek, J. I. Rodríguez, P. Romaniello, P. Ros, P. R. T. Schipper, G. Schreckenbach, J. S. Seldenthuis, M. Seth, D. G. Skachkov, J. G. Snijders, M. Solà, M. Swart, D. Swerhone, G. te Velde, P. Vernooijs, L. Versluis, L. Visscher, O. Visser, F. Wang, T. A. Wesolowski, E. M. van Wezenbeek, G. Wiesenekker, S. K. Wolff, T. K. Woo, A. L. Yakovlev, SCM, Amsterdam, **2010**.

[16] M. Swart, J. G. Snijders, *Theor. Chem. Acc.* **2003**, *110*, 34.
[17] E. van Lenthe, E. J. Baerends, J. G. Snijders, *J. Chem. Phys.* **1993**, *99*, 4597.
[18] E. J. Baerends, D. E. Ellis, P. Ros, *Chem. Phys.* **1973**, *2*, 41.
[19] S. H. Vosko, L. Wilk, M. Nusair, *Can. J. Phys.* **1980**, *58*, 1200.
[20] A. D. Becke, *Phys. Rev. A* **1988**, *38*, 3098.
[21] J. P. Perdew, *Phys. Rev. B* **1986**, *33*, 8822.
[22] M. Swart, M. Solà, F. M. Bickelhaupt, *J. Comput. Chem.* **2007**, *28*, 1551.
[23] M. Swart, F. M. Bickelhaupt, *J. Comput. Chem.* **2008**, *29*, 724.
[24] M. Swart, F. M. Bickelhaupt, *Int. J. Quantum Chem.* **2006**, *106*, 2536.
[25] S. K. Wolff, *Int. J. Quantum Chem.* **2005**, *104*, 645.
[26] a) R. C. Haddon, *J. Phys. Chem. A* **2001**, *105*, 4164; b) R. C. Haddon, S. Y. Chow, *J. Am. Chem. Soc.* **1998**, *120*, 10494.
[27] R. C. Haddon, *QCPE 508/QCMP 044*, QCPE Bull. **1988**, 8.
[28] a) S. Grimme, *J. Comput. Chem.* **2006**, *27*, 1787; b) S. Grimme, J. Antony, S. Ehrlich, H. Krieg, *J. Chem. Phys.* **2010**, *132*, 154104.
[29] S. Osuna, M. Swart, M. Solà, *J. Phys. Chem. A* **2011**, *115*, 3491.
[30] X. Wu, X. Lu, K. Tan, Q. Zhang, *J. Nanosci. Nanotechnol.* **2007**, *7*, 1346.
[31] A. Rodríguez-Fortea, N. Alegret, A. L. Balch, J. M. Poblet, *Nat. Chem.* **2010**, *2*, 955.
[32] Y. Li, K. N. Houk, *J. Am. Chem. Soc.* **1993**, *115*, 7478.
[33] S. Osuna, K. N. Houk, *Chem. Eur. J.* **2009**, *15*, 13219.
[34] W.-J. van Zeist, F. M. Bickelhaupt, *Org. Biomol. Chem.* **2010**, *8*, 3118.
[35] a) D. H. Ess, K. N. Houk, *J. Am. Chem. Soc.* **2007**, *129*, 10646; b) D. H. Ess, K. N. Houk, *J. Am. Chem. Soc.* **2008**, *130*, 10187.

Received: November 24, 2011
Revised: February 13, 2011
Published online: April 19, 2012

